J. Fluid Mech. (1980), *vol.* 99, *part* 4, *pp.* 755–783
Printed in Great Britain

A strong interaction theory for the creeping motion of a sphere between plane parallel boundaries. Part 2. Parallel motion

By PETER GANATOS, ROBERT PFEFFER AND SHELDON WEINBAUM

The City College of The City University of New York, New York 10031

(Received 19 October 1979 and in revised form 15 February 1980)

Exact solutions are presented for the three-dimensional creeping motion of a sphere of arbitrary size and position between two plane parallel walls for the following conditions: (*a*) pure translation parallel to two stationary walls, (*b*) pure rotation about an axis parallel to the walls, (*c*) Couette flow past a rigidly held sphere induced by the motion of one of the boundaries and (*d*) two-dimensional Poiseuille flow past a rigidly held sphere in a channel. The combined analytic and numerical solution procedure is the first application for bounded flow of the three-dimensional boundary collocation theory developed in Ganatos, Pfeffer & Weinbaum (1978). The accuracy of the solution technique is tested by detailed comparison with the exact bipolar co-ordinate solutions of Goldman, Cox & Brenner (1967*a*, *b*) for the drag and torque on a sphere translating parallel to a single plane wall, rotating adjacent to the wall or in the presence of a shear field. In all cases, the converged collocation solutions are in perfect agreement with the exact solutions for all spacings tested. The new collocation solutions have also been used to test the accuracy of existing solutions for the motion of a sphere parallel to two walls using the method of reflexions technique. The first-order reflexion theory of Ho & Leal (1974) provides reasonable agreement with the present results for the drag when the sphere is five or more radii from both walls. At closer spacings first-order reflexion theory is highly inaccurate and predicts an erroneous direction for the torque on the sphere for a wide range of sphere positions. Comparison with the classical higher-order method of reflexions solutions of Faxen (1923) reveals that the convergence of the multiple reflexion series solution is poor when the sphere centre is less than two radii from either boundary.

Solutions have also been obtained for the fluid velocity field. These solutions show that, for certain wall spacings and particle positions, a separated region of closed streamlines forms adjacent to the sphere which reverses the direction of the torque acting on a translating sphere.

1. Introduction

In this part 2 of the study we present the first application of the three-dimensional boundary collocation theory developed in Ganatos, Pfeffer & Weinbaum (1978) for strongly interacting spheres to bounded creeping-motion problems with planar symmetry. To illustrate the solution procedure we have selected an unsolved Stokes

0022-1120/80/4508-1720 $02.00

flow problem of long-standing interest, the slow longitudinal motion of a spherical particle of arbitrary size and position between two infinite plane parallel boundaries. The corresponding problem for the transverse motion of a sphere between two parallel walls has been treated in part 1, Ganatos, Weinbaum & Pfeffer (1980). Some recent biological and engineering applications where this flow geometry is important are described in the introduction of this previous paper.

The earliest theoretical treatment of the three-dimensional longitudinal flow situation was presented by Faxen (1923), details of which are given in Happel & Brenner (1973, pp. 322–327). Faxen considered the problem of a sphere translating between two parallel walls for the special cases where the sphere is either moving along the centre-line or in a plane at one-quarter the distance between the two walls. Faxen obtained expressions for the force and torque acting on the sphere by the method of reflexions using the five leading terms in the iterative series solution. This iterative method, which alternately satisfies boundary conditions on the sphere and on the infinite plane walls, gives accurate results only if both walls are sufficiently far removed from the surface of the sphere. The present solutions show that, at close particle-to-wall spacings, the higher-order interaction effects become significant and the leading terms of the iterative series give a poor description of the particle–wall interactions. Wakiya (1956) used a similar approach to treat the problem of a rigidly held sphere in Couette flow or two-dimensional Poiseuille flow. Wakiya's solution is also only for the case where the sphere is at one-quarter the distance between the walls.

The simpler flow situation of the rotation and translation of a sphere parallel to a single plane wall or in the presence of a linear shear field has been carefully examined by Goldman, Cox & Brenner (1967*a*, *b*). The exact solution method used by these authors for a single wall, however, cannot be applied when two walls are present since the solution is based on the limiting case of a spherical bipolar series expansion first introduced by O'Neill (1964) in which one of the spheres is taken as infinitely large. Halow & Wills (1970) simply added the contribution of two individual walls in order to obtain an estimate of the force acting on a sphere at any position between the two walls. At best, this approach gives only a first-order approximation to the true drag on the sphere and is incapable of predicting higher-order effects such as the formation of separated regions of closed streamlines which occur in the presence of two walls.

The most complete study to date of the two-wall problem is the work of Ho & Leal (1974). These authors used a perturbation method to study the lateral migration of a neutrally buoyant rigid sphere due to weak inertia effects when suspended in a fluid which is undergoing either simple shear flow or two-dimensional Poiseuille flow between two infinite plane boundaries. Their zeroth-order perturbation solution, which corresponds to the inertia-free Stokes flow solution, was obtained by the method of reflexions using two reflected fields. Solutions are presented for the motion of a sphere both parallel and perpendicular to the two plane walls at an arbitrary position between them. For the transverse flow problem it has been shown in part 1 of this investigation that the first two terms of the iterative series solution provide a reasonable description only if the sphere is at least five radii removed from each boundary.

This paper is presented in five sections. Section 2 contains the formulation for translation or rotation of a sphere along an axis parallel to two plane walls in the presence of a unidirectional flow between the walls. In § 3, the solution obtained in

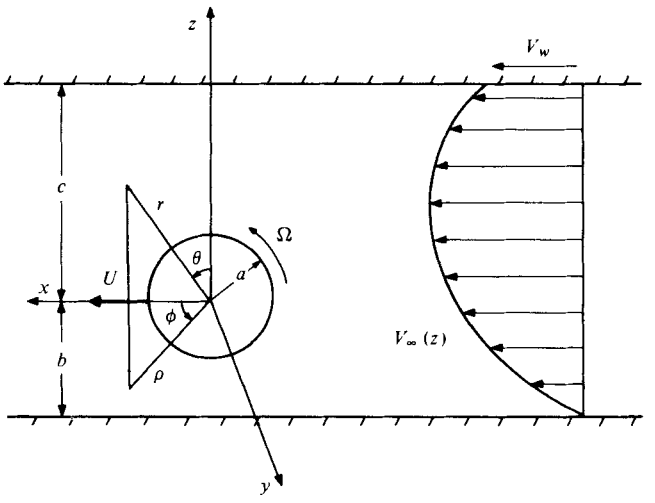

FIGURE 1. Geometry for the asymmetric flow configuration.

§ 2 is compared with exact published results of Goldman *et al.* (1967*a*, *b*) for the limiting case of a single wall. Solutions for the force and torque acting on the sphere in a variety of two-wall flow configurations are presented in § 4. Finally, § 5 contains some comments about the application of the solution technique in future research.

2. Mathematical formulation

In this section, the formulation will be presented for the following basic asymmetric flow problems involving a sphere of arbitrary size and position between two infinite plane parallel boundaries:

(*a*) translation without rotation of the sphere parallel to two stationary walls;

(*b*) rotation without any translation of the sphere;

(*c*) shear flow past a rigidly held sphere induced by the motion of one of the boundaries parallel to itself;

(*d*) Poiseuille flow past a rigidly held sphere in a channel. Solutions for any combination of these motions may be obtained by a simple superposition of solutions. The resulting motion of the sphere when it is not rigidly held in place may also be readily obtained from these basic solutions.

The geometry of the flow configuration is shown in figure 1. A sphere of radius a moves parallel to the two confining walls with constant velocity U. The fluid motion far removed from the sphere is unidirectional and parallel to the walls. Bretherton (1962) has shown that, for such a unidirectional flow, there is no lateral force acting on the sphere in the Stokes flow limit. The equations of motion for the fluid are:

$$\mu\nabla^2\mathbf{V} = \nabla p, \quad \nabla.\mathbf{V} = 0. \tag{2.1a, b}$$

For the geometry of the problem at hand, it is convenient to introduce rectangular (x, y, z) and spherical (r, θ, ϕ) co-ordinate systems whose origins coincide at the sphere centre. The velocity field $\mathbf{V}$ is decomposed into three parts:

$$\mathbf{V} = \mathbf{V}_\infty + \mathbf{V}_s + \mathbf{V}_w. \tag{2.2}$$

The part $\mathbf{V}_\infty$ represents the unidirectional velocity profile between the two plates far removed from the sphere. This profile independently satisfies (2.1) and the no-slip boundary conditions on the walls. For Poiseuille flow

$$\mathbf{V}_\infty = -\frac{4V_c(z+b)(z-c)}{(b+c)^2}\hat{\mathbf{i}}, \tag{2.3a}$$

where V_c is the centre-line velocity. For the shear flow resulting when the wall at $z = c$ in motion

$$\mathbf{V}_\infty = S(z+b)\hat{\mathbf{i}}, \tag{2.3b}$$

where S represents the velocity gradient which is constant.

The part $\mathbf{V}_s$ represents an infinite series containing all the simply separable solutions of (2.1) in spherical co-ordinates which have planar symmetry about the plane $y = 0$ and vanish as $r \to \infty$. This solution, which is a special case of Lamb's (1945) spherical harmonic series representation, is derived in Ganatos *et al.* (1978), and has the form of a double series with indices m and n. For the problem at hand, in which translational motion of the sphere occurs only along the x-axis and rotation only about the y-axis, only terms containing $m = 1$ are needed to describe the spherical disturbances. Thus the required form of the spherical solution is

$$\mathbf{V}_s = u_s\hat{\mathbf{i}} + v_s\hat{\mathbf{j}} + w_s\hat{\mathbf{k}}, \tag{2.4}$$

where

$$u_s = \sum_{n=1}^{\infty}[A_nA_n' + B_nB_n' + C_nC_n'], \tag{2.5a}$$

$$v_s = \sum_{n=1}^{\infty}[A_nA_n'' + B_nB_n'' + C_nC_n''], \tag{2.5b}$$

$$w_s = \sum_{n=1}^{\infty}[A_nA_n''' + B_nB_n''' + C_nC_n'''], \tag{2.5c}$$

and

$$A_n' = \frac{1}{2r^n}[2n(2n-1)\sin\theta P_n^1(\zeta)\cos^2\phi + (n-2)P_{n-1}^2(\zeta)\cos 2\phi - n(n+1)(n-2)P_{n-1}(\zeta)], \tag{2.6a}$$

$$B_n' = -\frac{1}{2r^{n+2}}[P_{n+1}^2(\zeta)\cos 2\phi - n(n+1)P_{n+1}(\zeta)], \tag{2.6b}$$

$$C_n' = \frac{1}{2r^{n+1}}[P_n^2(\zeta)\cos 2\phi + n(n+1)P_n(\zeta)], \tag{2.6c}$$

$$A_n'' = \frac{1}{r^n}[n(2n-1)\sin\theta P_n^1(\zeta) + (n-2)P_{n-1}^2(\zeta)]\cos\phi\sin\phi, \tag{2.6d}$$

$$B_n'' = -\frac{1}{r^{n+2}}P_{n+1}^2(\zeta)\cos\phi\sin\phi, \tag{2.6e}$$

$$C_n'' = \frac{1}{r^{n+1}}P_n^2(\zeta)\cos\phi\sin\phi, \tag{2.6f}$$

$$A_n''' = \frac{1}{r^n}[n(2n-1)\zeta P_n^1(\zeta) - (n+1)(n-2)P_{n-1}^1(\zeta)]\cos\phi, \tag{2.6g}$$

$$B_n''' = -\frac{1}{r^{n+2}} n P_{n+1}^1(\zeta)\cos\phi, \tag{2.6h}$$

$$C_n''' = -\frac{1}{r^{n+1}} P_n^1(\zeta)\cos\phi. \tag{2.6i}$$

Here P_n^m is the associated Legendre function of order n and degree m and $\zeta = \cos\theta$. A_n, B_n and C_n are unknown constants which will be determined by satisfying the no-slip boundary conditions on the surface of the sphere in the presence of the confining walls.

The part $\mathbf{V}_w$ represents a double integral of all separable solutions of (2.1) in rectangular co-ordinates which produce finite velocities everywhere in the flow field and is given by the double Fourier integral

$$\mathbf{V}_w = u_w\hat{\mathbf{i}} + v_w\hat{\mathbf{j}} + w_w\hat{\mathbf{k}}, \tag{2.7}$$

where

$$u_w = \int_0^\infty\int_0^\infty D_1(\alpha,\beta,z)\cos\alpha x\cos\beta y\,d\alpha\,d\beta, \tag{2.8a}$$

$$v_w = \int_0^\infty\int_0^\infty D_2(\alpha,\beta,z)\sin\alpha x\sin\beta y\,d\alpha\,d\beta, \tag{2.8b}$$

$$w_w = \int_0^\infty\int_0^\infty D_3(\alpha,\beta,z)\sin\alpha x\cos\beta y\,d\alpha\,d\beta, \tag{2.8c}$$

$$D_1(\alpha,\beta,z) = \left[A^*\left(1+\frac{\alpha^2}{\kappa}z\right) - A^{**}\frac{\alpha\beta}{\kappa}z - A^{***}\alpha z\right]e^{\kappa z} + \left[B^*\left(1-\frac{\alpha^2}{\kappa}z\right) + B^{**}\frac{\alpha\beta}{\kappa}z - B^{***}\alpha z\right]e^{-\kappa z}, \tag{2.9a}$$

$$D_2(\alpha,\beta,z) = \left[-A^*\frac{\alpha\beta}{\kappa}z + A^{**}\left(1+\frac{\beta^2}{\kappa}z\right) + A^{***}\beta z\right]e^{\kappa z} + \left[B^*\frac{\alpha\beta}{\kappa}z + B^{**}\left(1-\frac{\beta^2}{\kappa}z\right) + B^{***}\beta z\right]e^{-\kappa z}, \tag{2.9b}$$

$$D_3(\alpha,\beta,z) = [A^*\alpha z - A^{**}\beta z + A^{***}(1-\kappa z)]e^{\kappa z} + [B^*\alpha z - B^{**}\beta z + B^{***}(1+\kappa z)]e^{-\kappa z}, \tag{2.9c}$$

and $\kappa^2 = \alpha^2+\beta^2$. Here, the starred A and B coefficients are unknown functions of separation variables α and β. By proper choice of these functions, $\mathbf{V}_w$ is capable of exactly cancelling the disturbances produced by the sphere along the two planar boundaries.

To assist the reader in following the rather lengthy theoretical development which follows we shall briefly outline the general solution procedure. We seek a solution, equation (2.2), where $\mathbf{V}_\infty$, $\mathbf{V}_s$ and $\mathbf{V}_w$ are given respectively by equations (2.3), (2.5) and (2.8), which satisfies appropriate viscous flow boundary conditions on the confining walls and the surface of the sphere. Each of the fundamental solutions already satisfies the governing equation (2.1) at each point in the flow field, the proper boundedness conditions at infinity and the requirements of planar symmetry. The next step, which is the crucial one in the solution procedure, is to satisfy analytically the no-slip boundary conditions on both infinite confining walls simultaneously for an arbitrary

disturbance representing a sphere of unspecified size, position and velocity. The importance of doing this analytically stems from the fact that, whereas boundary collocation techniques are relatively easy to employ for finite boundaries, such as the surface of a sphere, they are very difficult to apply to infinite domain boundaries. In essence, one wishes to determine the functions D_i, $i = 1, 2, 3$, in equation (2.9) which satisfy the no-slip conditions on the planar walls for an arbitrary set of sphere coefficients A_n, B_n and C_n in equation (2.5). To accomplish this one must first express the spherical disturbances in rectangular co-ordinates so that the boundary conditions can be applied on constant co-ordinate surfaces representing the planar walls, and then invert the double Fourier integral transform of this disturbance so as to exactly satisfy the no-slip conditions on these infinite surfaces. Once this inversion is performed and the D_i functions expressed in terms of the A_n, B_n and C_n, the integrals in equation (2.8) are evaluated and the unknown constants in the spherical series expansion determined so as to satisfy the sphere boundary conditions by the numerical boundary collocation scheme devised for three-dimensional spherical disturbances in Ganatos *et al.* (1978).

In accord with the above solution outline, spherical coordinates (r, θ, ϕ) are related to the rectangular system (x, y, z) and the general spherical disturbances (2.5) are expressed in the latter reference frame. The desired co-ordinate transformation is (see figure 1)

$$r = (x^2 + y^2 + z^2)^{\frac{1}{2}}, \tag{2.10a}$$

$$\theta = \cos^{-1}\left[\frac{z}{(x^2 + y^2 + z^2)^{\frac{1}{2}}}\right], \tag{2.10b}$$

$$\phi = \tan^{-1}\left(\frac{y}{x}\right). \tag{2.10c}$$

Application of the three boundary conditions $u = V_\infty$, $v = 0$ and $w = 0$ along the two walls yields

$$\left.\begin{aligned}
&\int_0^\infty \int_0^\infty D_1(\alpha, \beta, z_i) \cos \alpha x \cos \beta y \, d\alpha \, d\beta \\
&\quad = -\sum_{n=1}^{\infty} [A_n A_n'(x, y, z_i) + B_n B_n'(x, y, z_i) + C_n C_n'(x, y, z_i)], \\
&\int_0^\infty \int_0^\infty D_2(\alpha, \beta, z_i) \sin \alpha x \sin \beta y \, d\alpha \, d\beta \\
&\quad = -\sum_{n=1}^{\infty} [A_n A_n''(x, y, z_i) + B_n B_n''(x, y, z_i) + C_n C_n''(x, y, z_i)], \\
&\int_0^\infty \int_0^\infty D_3(\alpha, \beta, z_i) \sin \alpha x \cos \beta y \, d\alpha \, d\beta \\
&\quad = -\sum_{n=1}^{\infty} [A_n A_n'''(x, y, z_i) + B_n B_n'''(x, y, z_i) + C_n C_n'''(x, y, z_i)],
\end{aligned}\right\} \quad i = 1, 2, \tag{2.11}$$

where z_i, $i = 1, 2$, is the value of z at the two walls ($z_1 = -b$, $z_2 = c$). The right-hand sides of (2.11) represent the spherical disturbances as felt by the two planar boundaries. Equations (2.11) reveal that the unknown D_1, D_2 and D_3 functions evaluated

at the two walls are simply Fourier transforms of these disturbances. These equations may be inverted to give

$$\left.\begin{aligned} D_1(\alpha,\beta,z_i) &= -\frac{4}{\pi^2}\int_0^\infty\int_0^\infty \Big\{\sum_{n=1}^\infty [A_n A_n'(s,t,z_i)+B_n B_n'(s,t,z_i) \\ &\qquad +C_n C_n'(s,t,z_i)]\Big\}\cos\alpha s\cos\beta t\,ds\,dt, \\ D_2(\alpha,\beta,z_i) &= -\frac{4}{\pi^2}\int_0^\infty\int_0^\infty \Big\{\sum_{n=1}^\infty [A_n A_n''(s,t,z_i)+B_n B_n''(s,t,z_i) \\ &\qquad +C_n C_n''(s,t,z_i)]\Big\}\sin\alpha s\sin\beta t\,ds\,dt, \\ D_3(\alpha,\beta,z_i) &= -\frac{4}{\pi^2}\int_0^\infty\int_0^\infty \Big\{\sum_{n=1}^\infty [A_n A_n'''(s,t,z_i)+B_n B_n'''(s,t,z_i) \\ &\qquad +C_n C_n'''(s,t,z_i)]\Big\}\sin\alpha s\cos\beta t\,ds\,dt, \end{aligned}\right\} \quad i=1,2. \tag{2.12}$$

Analytic evaluation of the double integrals required in (2.12) for arbitrary n is based on expressing the associated Legendre function by its polynomial representation

$$P_n^m(\zeta) = \frac{(1-\zeta^2)^{\frac{1}{2}m}}{2^n}\sum_{q=0}^{[\frac{1}{2}n]}\frac{(-1)^q(2n-2q)!\,\zeta^{n-2q-m}}{q!(n-q)!\,(n-2q-m)!}. \tag{2.13}$$

Here the square bracket $[x]$ represents the largest whole integer which is less than or equal to x. Once this substitution is made, the first integration may be performed using the integral representations of the modified Bessel functions of the second kind. These representations are found in Erdelyi *et al.* (1954). The second integration, now involving Fourier transforms of modified Bessel functions of the second kind, may also be performed using results given in the above reference. The required results of these integrations are given below.

$$\begin{aligned} F_1(\alpha,\beta,z_i,n,m) &= \int_0^\infty\int_0^\infty \frac{1}{(s^2+t^2+z_i^2)^{\frac{1}{2}(n+1)}}\frac{P_n^m(z_i/(s^2+t^2+z_i^2)^{\frac{1}{2}})}{(s^2+t^2)^{\frac{1}{2}m}}\cos\alpha s\cos\beta t\,ds\,dt \\ &= \frac{\pi}{2}|z_i|\sum_{q=0}^{[\frac{1}{2}n]} S_{nmq}(z_i)\,(\kappa|z_i|)^{n-q-\frac{1}{2}}K_{n-q-\frac{1}{2}}(\kappa|z_i|), \end{aligned} \tag{2.14a}$$

$$\begin{aligned} F_2(\alpha,\beta,z_i,n,m) &= \int_0^\infty\int_0^\infty \frac{s^2}{(s^2+t^2+z_i^2)^{\frac{1}{2}(n+1)}}\frac{P_n^m(z_i/(s^2+t^2+z_i^2)^{\frac{1}{2}})}{(s^2+t^2)^{\frac{1}{2}m}}\cos\alpha s\cos\beta t\,ds\,dt \\ &= \frac{\pi}{2}|z_i|^3\sum_{q=0}^{[\frac{1}{2}n]} S_{nmq}(z_i)\,(\kappa|z_i|)^{n-q-\frac{3}{2}}[K_{n-q-\frac{3}{2}}(\kappa|z_i|) \\ &\qquad -\alpha^2 z_i^2(\kappa|z_i|)^{n-q-\frac{5}{2}}K_{n-q-\frac{5}{2}}(\kappa|z_i|)], \end{aligned} \tag{2.14b}$$

$$\begin{aligned} F_3(\alpha,\beta,z_i,n,m) &= \int_0^\infty\int_0^\infty \frac{st}{(s^2+t^2+z_i^2)^{\frac{1}{2}(n+1)}}\frac{P_n^m(z_i/(s^2+t^2+z_i^2)^{\frac{1}{2}})}{(s^2+t^2)^{\frac{1}{2}m}}\sin\alpha s\sin\beta t\,ds\,dt \\ &= \frac{\pi}{2}\alpha\beta|z_i|^5\sum_{q=0}^{[\frac{1}{2}n]} S_{nmq}(z_i)\,(\kappa|z_i|)^{n-q-\frac{5}{2}}K_{n-q-\frac{5}{2}}(\kappa|z_i|), \end{aligned} \tag{2.14c}$$

$$\begin{aligned} F_4(\alpha,\beta,z_i,n,m) &= \int_0^\infty\int_0^\infty \frac{s}{(s^2+t^2+z_i^2)^{\frac{1}{2}(n+1)}}P_n^m\left(\frac{z_i}{(s^2+t^2+z_i^2)^{\frac{1}{2}}}\right)\sin\alpha s\cos\beta t\,ds\,dt \\ &= \frac{\pi}{2}\alpha|z_i|^3\sum_{q=0}^{[\frac{1}{2}n]} S_{nmq}(z_i)\,(\kappa|z_i|)^{n-q-\frac{3}{2}}K_{n-q-\frac{3}{2}}(\kappa|z_i|), \end{aligned} \tag{2.14d}$$

where

$$S_{nmq}(z_i) = \frac{(2/\pi)^{\frac{1}{2}}}{(-2)^q q!(n-2q-m)!\, z_i^{n+m}} \tag{2.15}$$

and K_ν is the modified Bessel function of the second kind of order ν. Application of these results to (2.12) gives

$$\left.\begin{aligned} D_1(\alpha,\beta,z_i) &= \sum_{n=1}^{\infty} [A_n \mathscr{A}_n^*(\alpha,\beta,z_i) + B_n \mathscr{B}_n^*(\alpha,\beta,z_i) + C_n \mathscr{C}_n^*(\alpha,\beta,z_i)], \\ D_2(\alpha,\beta,z_i) &= \sum_{n=1}^{\infty} [A_n \mathscr{A}_n^{**}(\alpha,\beta,z_i) + B_n \mathscr{B}_n^{**}(\alpha,\beta,z_i) + C_n \mathscr{C}_n^{**}(\alpha,\beta,z_i)], \\ D_3(\alpha,\beta,z_i) &= \sum_{n=1}^{\infty} [A_n \mathscr{A}_n^{***}(\alpha,\beta,z_i) + B_n \mathscr{B}_n^{***}(\alpha,\beta,z_i) + C_n \mathscr{C}_n^{***}(\alpha,\beta,z_i)], \end{aligned}\right\} \quad i = 1, 2, \tag{2.16}$$

where the starred $\mathscr{A}_n$, $\mathscr{B}_n$ and $\mathscr{C}_n$ functions can be expressed in closed form in terms of the F_i integrals, equation (2.14), and are listed in appendix A. Equations (2.16) give the D_1, D_2 and D_3 functions evaluated at the two walls in terms of the as yet unknown spherical coefficients A_n, B_n and C_n. These functions may be obtained for any value of z by applying (2.9) at the two walls $z = -b, c$. This procedure generates six linear algebraic equations which may be solved simultaneously to yield the six unknown functions A^*, A^{**}, A^{***}, B^*, B^{**} and B^{***} contained in (2.9). Once this is done, these functions are substituted back into (2.9) to give the D_1, D_2 and D_3 functions at any value of z. The process is very tedious but straightforward. The final results are

$$\begin{aligned} D_1(\alpha,\beta,z) = {} & G_5(\eta) D_1(\alpha,\beta,-b) - G_5(\sigma) D_1(\alpha,\beta,c) \\ & + G_6(\sigma,\eta) \frac{\alpha}{K^2} [\alpha D_1(\alpha,\beta,-b) - \beta D_2(\alpha,\beta,-b)] \\ & - G_6(\eta,\sigma) \frac{\alpha}{K^2} [\alpha D_1(\alpha,\beta,c) - \beta D_2(\alpha,\beta,c)] \\ & + G_1(\sigma,\eta) \frac{\alpha}{K} D_3(\alpha,\beta,-b) \\ & - G_1(\eta,\sigma) \frac{\alpha}{K} D_3(\alpha,\beta,c), \end{aligned} \tag{2.17a}$$

$$\begin{aligned} D_2(\alpha,\beta,z) = {} & - G_6(\sigma,\eta) \frac{\alpha\beta}{K^2} \left[D_1(\alpha,\beta,-b) + \frac{\alpha}{\beta} D_2(\alpha,\beta,-b) \right] \\ & + G_6(\eta,\sigma) \frac{\alpha\beta}{K^2} \left[D_1(\alpha,\beta,c) + \frac{\alpha}{\beta} D_2(\alpha,\beta,c) \right] \\ & + G_3(\sigma,\eta) D_2(\alpha,\beta,-b) - G_3(\eta,\sigma) D_2(\alpha,\beta,c) \\ & - G_1(\sigma,\eta) \frac{\beta}{K} D_3(\alpha,\beta,-b) \\ & + G_1(\eta,\sigma) \frac{\beta}{K} D_3(\alpha,\beta,c), \end{aligned} \tag{2.17b}$$

$$D_3(\alpha,\beta,z) = G_2(\sigma,\eta)\left[\frac{\alpha}{\kappa}D_1(\alpha,\beta,-b)-\frac{\beta}{\kappa}D_2(\alpha,\beta,-b)\right]$$
$$-G_2(\eta,\sigma)\left[\frac{\alpha}{\kappa}D_1(\alpha,\beta,c)-\frac{\beta}{\kappa}D_2(\alpha,\beta,c)\right]$$
$$+G_4(\sigma,\eta)\,D_3(\alpha,\beta,-b)$$
$$-G_4(\eta,\sigma)\,D_3(\alpha,\beta,c), \tag{2.17c}$$

where

$$G_{1,2}(\mu,\nu) = 4\tau\mu\nu\left[\frac{\sinh\mu}{\mu}\pm\frac{\sinh\tau}{\tau}\frac{\sinh\nu}{\nu}\right]\Big/\delta_2, \tag{2.18a}$$

$$G_{3,4}(\mu,\nu) = 4\tau\left\{\nu\left[\cosh\mu-\frac{\sinh\tau}{\tau}\frac{\sinh\nu}{\nu}\right]\pm\mu\left[\frac{\sinh\mu}{\mu}-\frac{\sinh\tau}{\tau}\cosh\nu\right]\right\}\Big/\delta_2, \tag{2.18b}$$

$$G_5(\mu) = (-2\sinh\mu)/\delta_1, \tag{2.18c}$$

$$G_6(\mu,\nu) = 8\tau^2\left\{\mu\frac{\sinh\tau}{\tau}\left[\frac{\sinh\mu}{\mu}-\frac{\sinh\tau}{\tau}\cosh\nu\right]\right.$$
$$\left.+\nu\left[\frac{\sinh\tau}{\tau}\cosh\mu-\frac{\sinh\nu}{\nu}\right]\right\}\Big/\delta_1\delta_2. \tag{2.18d}$$

In the above equations, the subscripts 1, 3 and 2, 4 refer to the plus and minus signs on the right-hand sides, μ and ν are dummy variables,

$$\delta_1 = 2\sinh\tau, \quad \delta_2 = 4[\sinh^2\tau-\tau^2], \tag{2.19a, b}$$

$$\sigma = \kappa(z+b), \quad \eta = \kappa(z-c) \tag{2.20a, b}$$

and

$$\tau = \kappa(b+c). \tag{2.20c}$$

The expressions for the D_1, D_2 and D_3 functions, which are still in terms of the unknown spherical coefficients A_n, B_n and C_n, are substituted into (2.8) to yield $\mathbf{V}_w$.

The double integrals required in (2.8) cannot be performed analytically. However, instead of carrying out the integration for $0 \leqslant \alpha \leqslant \infty, 0 \leqslant \beta \leqslant \infty$ the substitution

$$\alpha = \kappa\cos\gamma, \quad \beta = \kappa\sin\gamma \tag{2.21a, b}$$

transforms (2.8) into

$$u_w = \int_0^\infty\int_0^{\frac{1}{2}\pi}\kappa D_1(\kappa,\gamma,z)\cos(\kappa x\cos\gamma)\cos(\kappa y\sin\gamma)\,d\gamma\,d\kappa, \tag{2.22a}$$

$$v_w = \int_0^\infty\int_0^{\frac{1}{2}\pi}\kappa D_2(\kappa,\gamma,z)\sin(\kappa x\cos\gamma)\sin(\kappa y\sin\gamma)\,d\gamma\,d\kappa, \tag{2.22b}$$

$$w_w = \int_0^\infty\int_0^{\frac{1}{2}\pi}\kappa D_3(\kappa,\gamma,z)\sin(\kappa x\cos\gamma)\cos(\kappa y\sin\gamma)\,d\gamma\,d\kappa, \tag{2.22c}$$

where the D_1, D_2 and D_3 functions are now functions of κ and γ. The advantage of this form is that the inner integration with respect to γ may be performed analytically using results for Fourier transforms found in Erdelyi *et al.* (1954). The required formulas are summarized in appendix B. The outer integrals with respect to κ must still be performed numerically.

After performing the integration with respect to γ and substituting (2.5) and (2.22) into (2.2), the following expressions for the local fluid velocity are obtained:

$$\mathbf{V} = u\hat{\mathbf{i}} + v\hat{\mathbf{j}} + w\hat{\mathbf{k}}, \tag{2.23}$$

where

$$\begin{aligned} u = V_\infty + \sum_{n=1}^{\infty} \{ & A_n[A_n'(x,y,z) + \mathscr{A}_n'(x,y,z)] \\ & + B_n[B_n'(x,y,z) + \mathscr{B}_n'(x,y,z)] \\ & + C_n[C_n'(x,y,z) + \mathscr{C}_n'(x,y,z)]\}, \end{aligned} \tag{2.24a}$$

$$\begin{aligned} v = \sum_{n=1}^{\infty} \{ & A_n[A_n''(x,y,z) + \mathscr{A}_n''(x,y,z)] \\ & + B_n[B_n''(x,y,z) + \mathscr{B}_n''(x,y,z)] \\ & + C_n[C_n''(x,y,z) + \mathscr{C}_n''(x,y,z)]\}, \end{aligned} \tag{2.24b}$$

$$\begin{aligned} w = \sum_{n=1}^{\infty} \{ & A_n[A_n'''(x,y,z) + \mathscr{A}_n'''(x,y,z)] \\ & + B_n[B_n'''(x,y,z) + \mathscr{B}_n'''(x,y,z)] \\ & + C_n[C_n'''(x,y,z) + \mathscr{C}_n'''(x,y,z)]\}. \end{aligned} \tag{2.24c}$$

Here the primed A_n, B_n and C_n functions are given by (2.6) and (2.10). The primed $\mathscr{A}_n$, $\mathscr{B}_n$ and $\mathscr{C}_n$ functions are somewhat lengthy and are listed in appendix C.

The solution (2.23) satisfies the no-slip boundary conditions all along the two walls for each value of the constant coefficients A_n, B_n and C_n. The integrals appearing in the primed $\mathscr{A}_n$, $\mathscr{B}_n$ and $\mathscr{C}_n$ functions in appendix C must be performed numerically using the Taylor series representation of the integrands for small values of κ to avoid round-off error and their asymptotic formulae for large values of κ to avoid machine overflows.

The boundary conditions remaining to be satisfied on the sphere surface, $r = a$, are

$$u = U, \quad v = 0, \quad w = 0, \tag{2.25a, b, c}$$

where U is the velocity with which the sphere is translating parallel to the walls. The collocation technique presented in Ganatos *et al.* (1978) may now be used for this purpose. At $r = a$, boundary conditions (2.25) are applied at M points on the surface of the sphere and the series solution (2.24) is truncated after M terms. This generates a system of $3M$ linear algebraic equations for the $3M$ unknown coefficients A_n, B_n and C_n of the spherical solution. The solution for the velocity field is completely known once these coefficients are determined.

The hydrodynamic force and torque acting on the sphere are found from Ganatos *et al.* (1978) to be

$$\mathbf{F} = -8\pi\mu A_1\hat{\mathbf{i}}, \quad \mathbf{T} = -8\pi\mu C_1\hat{\mathbf{j}}. \tag{2.26a, b}$$

Using the notation of Goldman *et al.* (1967*a*, *b*) for the four problems outlined at the beginning of this section, the force and torque acting on the sphere are given by

$$\mathbf{F} = 6\pi\mu a U F_x^t\hat{\mathbf{i}}, \quad \mathbf{T} = 8\pi\mu a^2 U T_y^t\hat{\mathbf{j}} \tag{2.27a, b}$$

for a sphere translating with velocity U in the x direction. For a sphere rotating with angular velocity Ω about the y axis

$$\mathbf{F} = 6\pi\mu a^2\Omega F_x^r \hat{\mathbf{i}}, \quad \mathbf{T} = 8\pi\mu a^3\Omega T_y^r \hat{\mathbf{j}}. \tag{2.28a, b}$$

For shear flow past a rigidly held sphere induced by the steady motion of the boundary at $z = c$,

$$\mathbf{F} = 6\pi\mu abSF_x^s \hat{\mathbf{i}}, \quad \mathbf{T} = 4\pi\mu a^3 S T_y^s \hat{\mathbf{j}}, \tag{2.29a, b}$$

while for Poiseuille flow past a rigidly held sphere between two stationary walls

$$\mathbf{F} = 6\pi\mu a V_c F_x^p \hat{\mathbf{i}}, \quad \mathbf{T} = 8\pi\mu a^2 V_c T_y^p \hat{\mathbf{j}}. \tag{2.30a, b}$$

The non-dimensional force and torque coefficients defined by (2.27)–(2.30) are found using (2.26), i.e.

$$F_x^t = -\frac{4}{3}\frac{A_1^t}{aU}, \quad T_y^t = -\frac{C_1^t}{a^2 U}, \tag{2.31a, b}$$

$$F_x^r = -\frac{4}{3}\frac{A_1^r}{a^2\Omega}, \quad T_y^r = -\frac{C_1^r}{a^3\Omega}, \tag{2.32a, b}$$

$$F_x^s = -\frac{4}{3}\frac{A_1^s}{abS}, \quad T_y^s = -\frac{2C_1^s}{a^3 S}, \tag{2.33a, b}$$

$$F_x^p = -\frac{4}{3}\frac{A_1^p}{aV_c}, \quad T_y^p = -\frac{C_1^p}{a^2 V_c}, \tag{2.34a, b}$$

where the A_1 and C_1 coefficients are determined from the collocation of (2.24) with the appropriate boundary conditions.

3. Solutions for the motion of a sphere parallel to a single plane wall

In this section, the accuracy and convergence characteristics of the collocation procedure applied to (2.24) will be tested by comparing solutions obtained by the present method with the exact results of Goldman *et al.* (1967*a*) for translation without rotation of a sphere parallel to a single plane wall and for rotation about an axis parallel to the wall without any translation and with the exact solutions of Goldman *et al.* (1967*b*) for shear flow past a rigidly held sphere in the presence of a single planar boundary.

For the purpose of making the comparison, the effect of the second wall may be removed from the more general two-wall solution presented in the previous section by taking the limit as $c \to \infty$. In this limit the G_i functions in equation (2.18) and the H_i functions in appendix C reduce to:

$$G_{1,2}(\sigma, \eta \to -\infty) = \mp\sigma e^{-\sigma}, \quad G_{1,2}(\eta \to -\infty, \sigma) = 0, \tag{3.1a, b}$$

$$G_{3,4}(\sigma, \eta \to -\infty) = (1 \mp \sigma) e^{-\sigma}, \quad G_{3,4}(\eta \to -\infty, \sigma) = 0, \tag{3.1c, d}$$

$$G_5(\eta \to -\infty) = e^{-\sigma}, \quad G_5(\sigma) = 0, \tag{3.1e, f}$$

$$G_6(\sigma, \eta \to -\infty) = -\sigma e^{-\sigma}, \quad G_6(\eta \to -\infty, \sigma) = 0; \tag{3.1g, h}$$

$$H_i(c \to \infty) = 0, \quad i = 1, \ldots, 24. \tag{3.2}$$

M	$\alpha = 0{\cdot}5$ $b/a = 1{\cdot}13$	$\alpha = 1{\cdot}0$ $b/a = 1{\cdot}54$	$\alpha = 1{\cdot}5$ $b/a = 2{\cdot}35$	$\alpha = 2{\cdot}0$ $b/a = 3{\cdot}76$	$\alpha = 3{\cdot}0$ $b/a = 10{\cdot}1$
	(*a*) *Convergence of* F_x^t *for single wall at various sphere-to-wall spacings*				
2	−1·705	−1·465	−1·285	−1·169	−1·059
4	−2·031	−1·560	−1·307	−1·174	−1·059
6	−2·121	−1·567	−1·308	−1·174	
8	−2·144	−1·567	−1·308		
10	−2·149				
12	−2·151				
14	−2·151				
Exact	−2·151	−1·567	−1·308	−1·174	−1·059
	(*b*) *Convergence of* T_y^t *for single wall at various sphere-to-wall spacings*				
2	0·04529	0·01200	0·002402	0·0004049	$8{\cdot}722 \times 10^{-6}$
4	0·06357	0·01336	0·002554	0·0004165	$8{\cdot}761 \times 10^{-6}$
6	0·07073	0·01455	0·002641	0·0004216	$8{\cdot}775 \times 10^{-6}$
8	0·07235	0·01464	0·002642	0·0004216	$8{\cdot}775 \times 10^{-6}$
10	0·07315	0·01465	0·002642		
12	0·07352	0·01465			
14	0·07365				
16	0·07370				
18	0·07371				
Exact	0·07372	0·01465	0·002642	0·0004216	$8{\cdot}774 \times 10^{-6}$
	(*c*) *Convergence of* F_x^r *for single wall at varicus sphere-to-wall spacings*				
2	0·2041	0·05588	0·01027	0·0001579	$3{\cdot}078 \times 10^{-5}$
4	0·1232	0·02229	0·003705	0·0005726	$1{\cdot}173 \times 10^{-5}$
6	0·1041	0·01978	0·003530	0·0005623	$1{\cdot}170 \times 10^{-5}$
8	0·09961	0·01956	0·003523	0·0005621	$1{\cdot}170 \times 10^{-5}$
10	0·09868	0·01954	0·003523	0·0005621	
12	0·09844	0·01953			
14	0·09836	0·01953			
16	0·09832				
18	0·09830				
Exact	0·09829	0·01953	0·003523	0·0005621	$1{\cdot}170 \times 10^{-5}$

TABLE 1

Careful examination of (2.24) shows that when the no-slip boundary conditions are applied on the surface of the sphere $r = a$, the solution of the coefficient matrix generated becomes independent of the ϕ co-ordinate of the boundary points. Thus, in contrast to the more general collocation procedure presented in Ganatos *et al.* (1978) in which the no-slip boundary conditions are satisfied at discrete points on the sphere surface, for the problem at hand, when the no-slip conditions are satisfied at the point $r = a$, $\theta =$ constant, $\phi =$ constant, the boundary conditions are actually satisfied on the ring $r = a$, $\theta =$ constant, $0 \leqslant \phi \leqslant 2\pi$. Thus in selecting the boundary points, any value of ϕ may be used except $\phi = 0$, $\frac{1}{2}\pi$ or π since the coefficient matrix becomes singular for these values.

The most advantageous collocation point to choose on the surface corresponding to the lowest-order truncation of the infinite series (2.24) is $\theta = \frac{1}{2}\pi$ since this point has the greatest control of the projected area of the sphere normal to its direction of

M	$\alpha = 0{\cdot}5$, $b/a = 1{\cdot}13$	$\alpha = 1{\cdot}0$, $b/a = 1{\cdot}54$	$\alpha = 1{\cdot}5$, $b/a = 2{\cdot}35$	$\alpha = 2{\cdot}0$, $b/a = 3{\cdot}76$	$\alpha = 3{\cdot}0$, $b/a = 10{\cdot}1$
	(*d*) *Convergence of* T_y^r *for single wall at various sphere-to-wall spacings*				
2	−1·205	−1·079	−1·023	−1·006	−1·000
4	−1·346	−1·099	−1·025	−1·006	−1·000
6	−1·380	−1·100	−1·025		
8	−1·387	−1·100			
10	−1·388				
12	−1·388				
Exact	−1·388	−1·100	−1·025	−1·006	−1·000
	(*e*) *Convergence of* F_x^s *for single wall at various sphere-to-wall spacings*				
2	1·514	1·392	1·262	1·163	1·059
4	1·614	1·438	1·278	1·167	1·059
6	1·616	1·439	1·278	1·167	
8	1·616	1·439			
Exact	1·616	1·439	1·278	1·167	1·059
	(*f*) *Convergence of* T_y^s *for single wall at various sphere-to-wall spacings*				
2	0·9799	0·9811	0·9913	0·9972	0·9998
4	0·9548	0·9748	0·9903	0·9971	0·9998
6	0·9535	0·9742	0·9901	0·9771	
8	0·9537	0·9742	0·9901		
10	0·9537				
Exact	0·9537	0·9742	0·9901	0·9971	0·9998

TABLE 1 (*continued*)

motion and also satisfies the no-slip boundary conditions exactly on the largest ring around the sphere. Unfortunately, the coefficient matrix becomes singular if this point is used. Convergence trials for the force and torque coefficients were performed using two adjacent points $\theta = \frac{1}{2}\pi \pm \epsilon$ as $\epsilon \to 0$. Tables presenting the results of these tests are contained in Ganatos (1979) and will not be repeated here. Convergence for all six coefficients to five significant figures was obtained for $\epsilon \leqslant 0{\cdot}01°$ at all spacings tested. Additional points are selected as mirror-image pairs about the plane $\theta = \frac{1}{2}\pi$.

In the first scheme used for spacing the additional boundary points, the semi-circular arc $r = a$, $0 \leqslant \theta \leqslant \pi$, $\phi =$ constant was divided into equal segments (e.g., for $M = 6$, $\theta = 30$, 60, 89·99, 90·01, 120, 150°). Solutions for the force and torque coefficients with increasing M at various spacings are compared with the exact results of Goldman *et al.* (1967*a*, *b*) in table 1. The bipolar co-ordinate parameter α used by these authors is related to the sphere–wall spacing via $\alpha = \cosh^{-1}(b/a)$. Convergence of F_x^t, T_y^r, F_x^s and T_y^s is quickly achieved to four significant digits at all spacings tested and solutions obtained are in perfect agreement with exact values. Solutions for T_y^t and F_x^r are within 0·01 % of the exact solutions at the closest spacing $\alpha = 0{\cdot}5$ ($b/a = 1{\cdot}13$) for $M = 18$ and in perfect agreement with the exact solutions at all other spacings. Unfortunately, the execution time required to obtain solutions for $M > 18$ (more than 35 min on an AMDAHL 470/V6 computer) was prohibitively long. The error in the last digit of the converged value of T_y^t for $\alpha = 3$ is believed to be due to round-off error.

At this point it would be of interest to determine how placing a boundary point

M	$\alpha = 0{\cdot}5$ $b/a = 1{\cdot}13$	$\alpha = 1{\cdot}0$ $b/a = 1{\cdot}54$	$\alpha = 1{\cdot}5$ $b/a = 2{\cdot}35$	$\alpha = 2{\cdot}0$ $b/a = 3{\cdot}76$	$\alpha = 3{\cdot}0$ $b/a = 10{\cdot}1$
	(*a*) *Convergence of* F_x^t *for single wall at various sphere-to-wall spacings*				
4	−4·084	−1·598	−1·310	−1·174	−1·059
6	−2·176	−1·567	−1·308	−1·174	−1·059
8	−2·140	−1·567	−1·308		
10	−2·148				
12	−2·151				
14	−2·151				
Exact	−2·151	−1·567	−1·308	−1·174	−1·059
	(*b*) *Convergence of* T_y^t *for single wall at various sphere-to-wall spacings*				
4	−0·3807	0·01118	0·002478	0·0004118	$8{\cdot}747 \times 10^{-6}$
6	0·08567	0·01504	0·002651	0·0004218	$8{\cdot}775 \times 10^{-6}$
8	0·07882	0·01465	0·002642	0·0004216	$8{\cdot}775 \times 10^{-6}$
10	0·07518	0·01465	0·002642	0·0004216	
12	0·07398				
14	0·07375				
16	0·07372				
18	0·07372				
Exact	0·07372	0·01465	0·002642	0·0004216	$8{\cdot}774 \times 10^{-6}$
	(*c*) *Convergence of* F_x^r *for single wall at various sphere-to-wall spacings*				
4	−2·547	0·0009137	0·002677	0·0005181	$1{\cdot}159 \times 10^{-5}$
6	0·09606	0·02017	0·003536	0·0005624	$1{\cdot}170 \times 10^{-5}$
8	0·1116	0·01956	0·003523	0·0005621	$1{\cdot}170 \times 10^{-5}$
10	0·1017	0·01953	0·003523	0·0005621	
12	0·09893	0·01953			
14	0·09839				
16	0·09830				
18	0·09829				
Exact	0·09829	0·01953	0·003523	0·0005621	$1{\cdot}170 \times 10^{-5}$

TABLE 2

near the wall $\theta = 0, \pi$ would affect the rate of convergence especially at close spacings. The singularity of the coefficient matrix at $\theta = 0, \pi$ is avoided by using the points $\theta = \epsilon, \frac{1}{2}\pi \pm \epsilon, \pi - \epsilon$ and taking the limit as $\epsilon \to 0$ until convergence is achieved to the desired number of digits. Again, convergence to five significant digits was achieved for all spacings for $\epsilon \leqslant 0{\cdot}01°$. With additional points equally spaced along the arc $0 < \theta < \pi$ on the sphere (e.g., for $M = 6$, $\theta = 0{\cdot}01$, 45, 89·99, 90·01, 135, 179·99°), the rate of convergence with increasing M is examined in table 2. In contrast to the case of a sphere translating perpendicular to a single plane wall, Ganatos, Weinbaum & Pfeffer (1980), where a similar collocation scheme was used and the rate of convergence of the drag coefficient was accelerated, comparison of table 2 (*a*) with table 1 (*a*) shows no change in the rate of convergence in F_x^t. This behaviour may be explained by the fact that for a sphere moving perpendicular to a wall rather large fluid velocities can be generated in the intervening fluid gap when its dimensions become smaller than the sphere radius. The inclusion of boundary points on the surface of the sphere in the region of close apposition for the transverse motion therefore can significantly improve the description of the flow field. On the other hand, the flow velocities produced by a sphere translating parallel to a wall are of the same order as the sphere

M	$\alpha = 0{\cdot}5$, $b/a = 1{\cdot}13$	$\alpha = 1{\cdot}0$, $b/a = 1{\cdot}54$	$\alpha = 1{\cdot}5$, $b/a = 2{\cdot}35$	$\alpha = 2{\cdot}0$, $b/a = 3{\cdot}76$	$\alpha = 3{\cdot}0$, $b/a = 10{\cdot}1$
	(*d*) *Convergence of* T_y^r *for single wall at various sphere-to-wall spacings*				
4	−2·265	−1·107	−1·025	−1·006	−1·000
6	−1·378	−1·099	−1·025	−1·006	−1·000
8	−1·381	−1·100			
10	−1·386	−1·100			
12	−1·387				
14	−1·388				
16	−1·388				
Exact	−1·388	−1·100	−1·025	−1·006	−1·000
	(*e*) *Convergence of* F_x^s *for single wall at various sphere-to-wall spacings*				
4	1·632	1·442	1·279	1·167	1·059
6	1·616	1·439	1·278	1·167	1·059
8	1·616	1·439	1·278		
Exact	1·616	1·439	1·278	1·167	1·059
	(*f*) *Convergence of* T_y^s *for single wall at various sphere-to-wall spacings*				
4	0·9580	0·9730	0·9903	0·9971	0·9998
6	0·9539	0·9743	0·9901	0·9971	0·9998
8	0·9535	0·9742	0·9901		
10	0·9537	0·9742			
12	0·9537				
Exact	0·9537	0·9742	0·9901	0·9971	0·9998

TABLE 2 (*continued*)

velocity and concentrating the boundary points near the wall has little effect on the rate of convergence of the solution. In fact, comparison of tables 2(*d*)–(*f*) with tables 1(*d*)–(*f*) shows that concentrating boundary points on the surface of the sphere near the wall actually has a small adverse effect on the rate of convergence of the coefficients T_y^r, F_x^s and T_y^s while slightly improving the rate of convergence of T_y^t and F_x^r. The collocation scheme used in table 2 allows convergence of all six force and torque coefficients to the exact solution to four significant figures with $M \leqslant 18$ at all spacings tested. Convergence is achieved to four significant figures with $M \geqslant 10$ at $\alpha = 1{\cdot}0$ ($b/a = 1{\cdot}54$), $M \geqslant 8$ at $\alpha = 2$ ($b/a = 3{\cdot}76$) and $M \geqslant 6$ at $\alpha = 3{\cdot}0$ ($b/a = 10{\cdot}1$). The converged value of T_y^t for $\alpha = 3$ is the same as that obtained using the first collocation scheme in table 1.

In light of the above numerical results, the second collocation scheme used in table 2 in which boundary points are placed near $\theta = 0, \pi$ is slightly more efficient when computing all of the force and torque coefficients simultaneously and will be used in the remainder of this study.

4. Solutions for the motion of a sphere parallel to two plane walls

In this section, collocation solutions involving two walls will be presented for the four problems outlined at the beginning of §2. To the best of the authors' knowledge, the only solutions available for these two-wall problems were obtained by the approximate method of reflexions technique.

A number of formulae for the various force and torque coefficients have been obtained by method of reflexions techniques for special configurations involving a sphere between two plane parallel walls. These formulae are summarized in Happel & Brenner (1973, pp. 322–329). For the purpose of comparison, the relevant formulae will now be presented.

The position parameter s is defined as the ratio b/d where $d = b + c$ (see figure 1). For $s = 0{\cdot}25$, i.e. when the centre of the sphere is located at $\frac{1}{4}$ of the distance between the two walls, Faxen (1923) obtained the formulae for pure translation

$$F_x^t = -\frac{1}{1-0{\cdot}6526(a/b)+0{\cdot}1475(a/b)^3-0{\cdot}131(a/b)^4-0{\cdot}0644(a/b)^5}, \tag{4.1}$$

$$T_y^t = -\frac{0{\cdot}025(a/b)^2}{1-0{\cdot}6526(a/b)}, \tag{4.2}$$

while for $s = 0{\cdot}5$ he obtained

$$F_x^t = -\frac{1}{1-1{\cdot}004(a/b)+0{\cdot}418\,(a/b)^3+0{\cdot}21(a/b)^4-0{\cdot}169\,(a/b)^5}. \tag{4.3}$$

For $s = 0{\cdot}25$ Wakiya (1956) obtained the following formulae for a rigidly held sphere in shear and Poiseuille flow respectively:

$$F_x^s = \frac{1}{1-0{\cdot}6526(a/b)+0{\cdot}4003(a/b)^3-0{\cdot}297(a/b)^4}, \tag{4.4}$$

$$T_y^s = 1+0{\cdot}0506(a/b)+0{\cdot}033(a/b)^2; \tag{4.5}$$

$$F_x^p = \frac{\frac{3}{4}[1-\frac{1}{9}(a/b)^2]}{1-0{\cdot}6526(a/b)+0{\cdot}3160(a/b)^3-0{\cdot}242(a/b)^4}, \tag{4.6}$$

$$T_y^p = \tfrac{1}{4}(a/b)\,[1+0{\cdot}0758(a/b)+0{\cdot}049(a/b)^2]. \tag{4.7}$$

The predictions of Faxen's formulae are compared with the present collocation solutions and the weak interaction method of reflexions results of Ho & Leal (1974) in figures 2(a, b). Figure 2(a) shows a comparison of solutions for the drag on a sphere translating parallel to two plane walls. The solid lines represent the converged collocation solutions which are in perfect agreement with the exact single-wall results of Goldman *et al.* (1967a) ($s = 0$). The weak interaction method of reflexions results of Ho & Leal (1974) give considerable error over the entire range of s. At $b/a = 1{\cdot}1$ the value of the drag predicted by the weak interaction theory of Ho & Leal is as much as 50 % below the true value. At $b/a = 2$ the error is as high as 20 %. It is only for spacings of $b/a \geqslant 5$ that the weak interaction theory gives reasonably accurate results. At $s = 0{\cdot}25$, Faxen's result (equation (4.1)), which includes the effect of three additional terms in the iterative series, is in good agreement with the collocation theory. However, when $s = 0{\cdot}5$ (equation (4.3)) even this more accurate solution breaks down and gives an error as high as 40 % at $b/a = 1{\cdot}1$.

Figure 2(b) shows similar results for the torque on a sphere translating parallel to two plane walls. When $s = 0$ the converged collocation solutions are in excellent agreement with the exact single-wall results of Goldman *et al.* (1967a) at all values of b/a. For $b/a \geqslant 5$ the weak interaction theory of Ho & Leal (1974) is in very good agreement with the collocation theory for $0{\cdot}2 \leqslant s \leqslant 0{\cdot}5$. For smaller values of s, as the second wall is moved further away from the sphere, the weak interaction theory

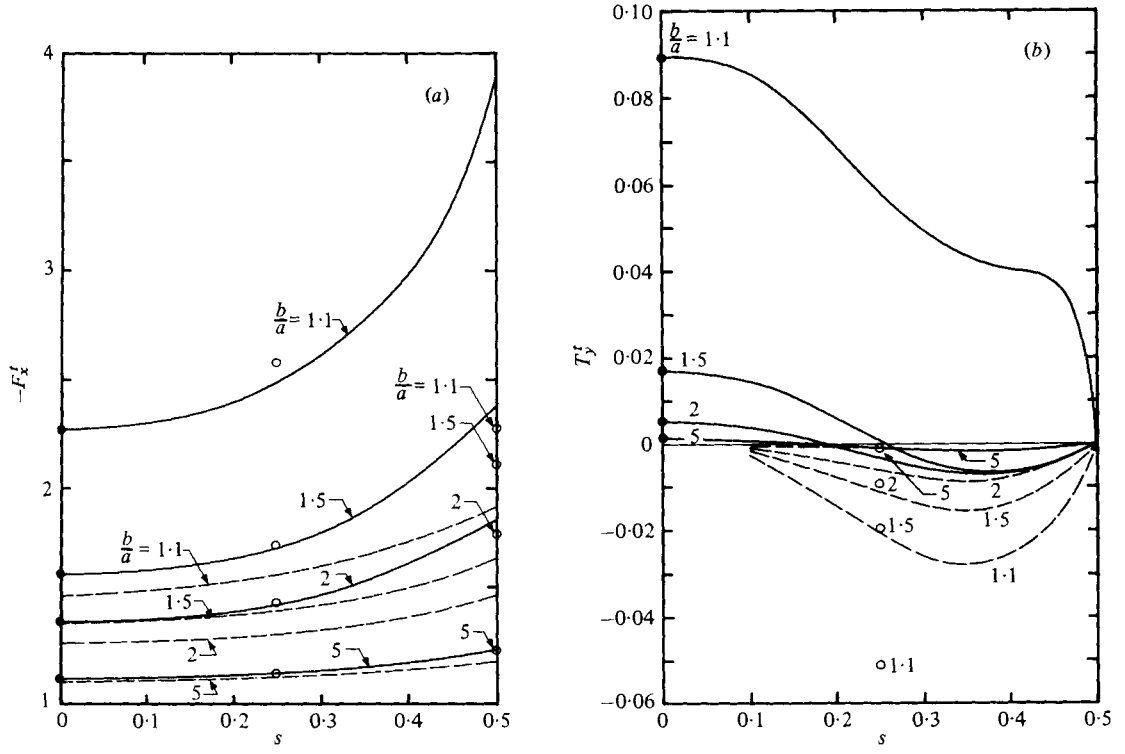

FIGURE 2. Comparison of solutions for (*a*) the drag and (*b*) the torque on a sphere translating parallel to two plane walls. ——, collocation (present study); - - - - -, Ho & Leal (1974), weak interaction method of reflexions; ○, Faxen (1923), equations (4.1)–(4.3); ●, Goldman, Cox & Brenner (1967*a*), exact.

fails to predict the change in sign of the torque resulting from the increasing importance of the closer wall. For the special case of $s = 0{\cdot}25$ Faxen's result (equation (4.2)) is in good agreement with the collocation theory for $b/a \geqslant 5$, but, for reasons which are not evident, provides an improvement over the first-order reflexion results of Ho & Leal for the torque only when $b/a > 10$.

Table 3 shows a comparison between collocation solutions and results obtained using Wakiya's formulae (equations (4.4)–(4.7)) for the force and torque coefficients in Couette flow or two-dimensional Poiseuille flow for the special case $s = 0{\cdot}25$. At large values of b/a, agreement between the two theories is excellent. At closer spacings there is a gradual decay in the accuracy of the solutions obtained by the method of reflexions. At $b/a = 1{\cdot}1$ the error incurred in using Wakiya's formulae for F_x^s, T_y^s, F_x^p and T_y^p is relatively small, 4, 3, 5 and 8 % respectively for this particular value of s.

A serious practical limitation in obtaining the asymmetric bounded-flow solutions contained herein is the computation time required to generate the coefficient matrix (2.5). Computer running times for the two-wall asymmetric configurations were found to vary approximately as $(5\text{–}15)M^2$ seconds on an AMDAHL 470/V6 computer which is roughly one order of magnitude higher than for the corresponding axisymmetric case where the sphere is translating perpendicular to the walls (Ganatos *et al.* 1980). There are three reasons for the increase in computation time. First, because

b/a	Collocation theory	Wakiya (1956), equation (4.4)
	(*a*) F_x^s	
1·1	1·900	1·982
1·25	1·758	1·782
1·5	1·599	1·600
2·0	1·420	1·418
3·0	1·261	1·260
4·0	1·188	1·188
8·0	1·088	1·088
	(*b*) T_y^s	
1·1	1·039	1·073
1·25	1·034	1·061
1·5	1·028	1·048
2·0	1·023	1·034
3·0	1·017	1·021
4·0	1·013	1·015
8·0	1·007	1·007
	(*c*) F_x^p	
1·1	1·347	1·422
1·25	1·261	1·289
1·5	1·161	1·167
2·0	1·044	1·045
3·0	0·9364	0·9362
4·0	0·8858	0·8858
8·0	0·8147	0·8147
	(*d*) T_y^p	
1·1	0·2333	0·2521
1·25	0·2058	0·2184
1·5	0·1718	0·1787
2·0	0·1287	0·1313
3·0	0·08531	0·08589
4·0	0·06368	0·06388
8·0	0·03156	0·03157

TABLE 3. Comparison of values for force and torque coefficients obtained by the present collocation technique to values obtained by Wakiya (1956) for $s = 0{\cdot}25$.

there are three no-slip boundary conditions to be satisfied at each boundary point and three sets of unknown coefficients to be determined instead of two, the number of matrix elements (and the number of numerical integrations to be performed per run) increases from $4M^2$ to $9M^2$. Second, the expressions for the integrals in the asymmetric case (see appendix C) are considerably more complicated than the corresponding integrals for the axisymmetric case. Finally, since some of the force and torque

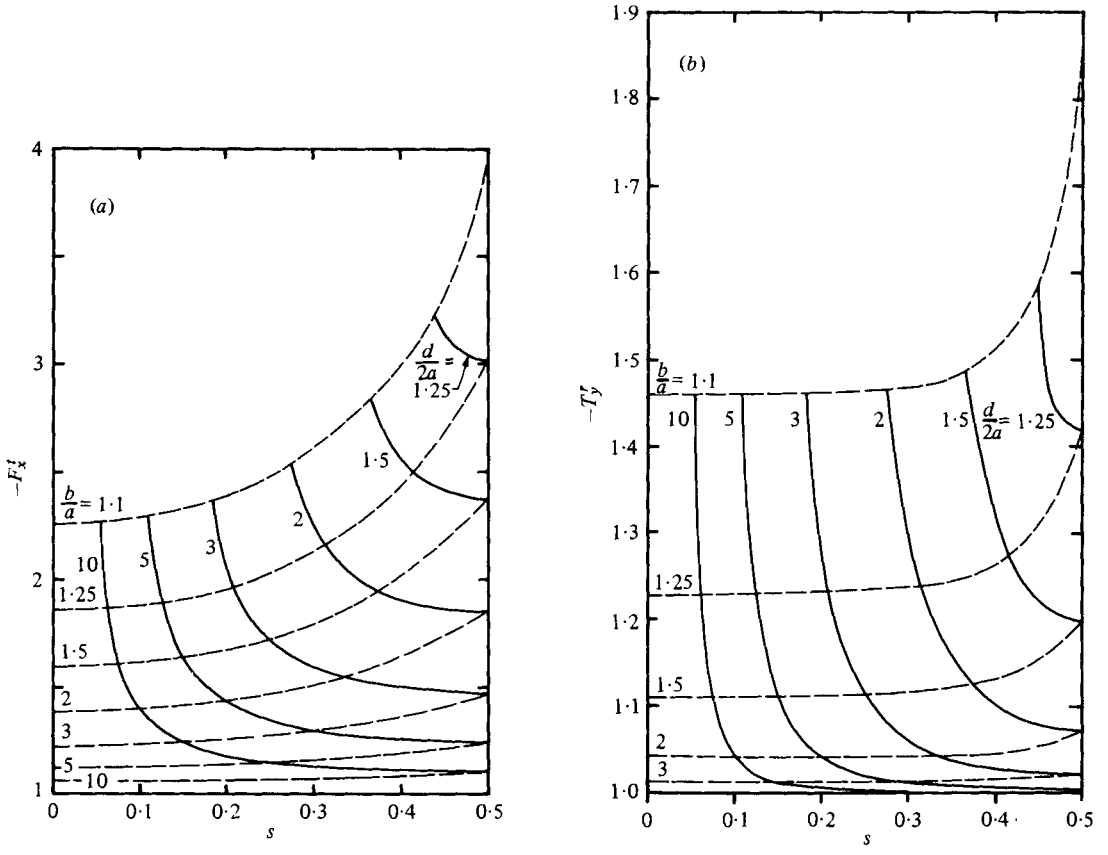

FIGURE 3(*a*, *b*). For legend see p. 774.

coefficients in the asymmetric case are small in magnitude, the numerical integrations must be carried out with a tighter tolerance in order to compute these coefficients accurately.

It should be noted that, since the primed coefficients in (2.24) depend only on the geometry and not on the boundary conditions satisfied on the sphere or V_∞, the force and torque coefficients (2.31)–(2.34) may be determined in a single computer run for a given geometry for all four of the problems outlined at the beginning of § 2. A further reduction in the number of computer runs required may be made by computing the force and torque coefficients at position $1-s$ using the results at position s by taking advantage of relations:

$$F_x^t(1-s) = F_x^t(s), \tag{4.8a}$$

$$T_y^t(1-s) = -T_y^t(s); \tag{4.8b}$$

$$F_x^r(1-s) = -F_x^r(s), \tag{4.9a}$$

$$T_y^r(1-s) = T_y^r(s); \tag{4.9b}$$

$$F_x^s(1-s) = -\frac{1}{1-s}[sF_x^s(s)+F_x^t(s)], \tag{4.10a}$$

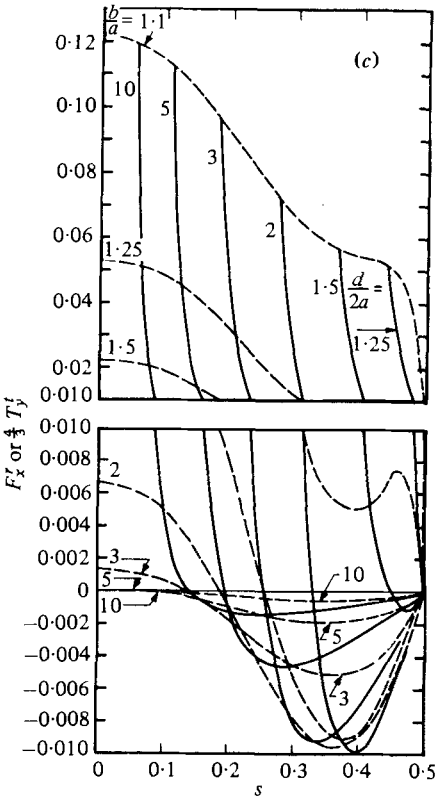

FIGURE 3. (*a*) Force on a sphere translating parallel to two plane walls. (*b*) Torque on a sphere rotating about an axis parallel to two plane parallel walls. (*c*) Force on a sphere rotating about an axis parallel to two plane walls or torque on a sphere translating parallel to two plane walls. ——, $d/2a$ = constant; - - - - -, b/a = constant.

$$T_y^s(1-s) = T_y^s(s) + \frac{2d}{a} T_y^t(s); \tag{4.10b}$$

$$F_x^p(1-s) = F_x^p(s); \tag{4.11a}$$

$$T_y^p(1-s) = -T_y^p(s). \tag{4.11b}$$

Figures 3, 5 and 6 present converged values of the force and torque coefficients defined by equations (2.27)–(2.30) at various spacings and as a function of sphere position s. The dashed lines show the effect of the position of the wall at $z = c$ for various sphere-to-wall spacings b/a. The solid lines show the variation of the force and torque cofficients as a function of particle position at various fixed wall-to-wall spacings $d/2a$. Figure 3 (*a*) shows the force acting on a sphere translating in a quiescent fluid parallel to two plane walls. At a given wall-to-wall spacing $d/2a$, the sphere experiences minimum drag when it is located midway between the two walls. The drag becomes infinite as the sphere approaches either of the walls. The non-zero slope of the dashed lines (b/a = constant) over most of the range of s demonstrates the effect that the presence of the second wall has on the drag of the sphere.

Figure 3 (*b*) shows the torque acting on a sphere which is rotating about an axis parallel to the walls. The behaviour of the torque on a rotating sphere is somewhat

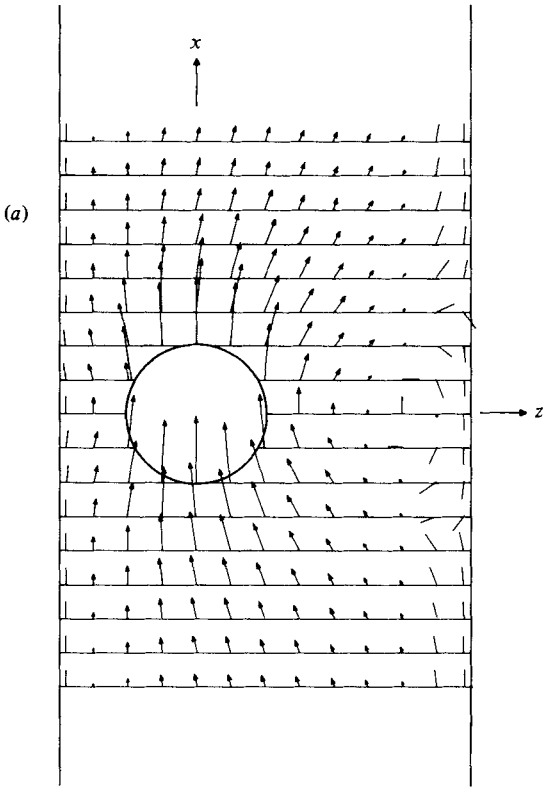

FIGURE 4(*a*). For legend see p. 776.

similar to the behaviour of the force on a translating sphere (see figure 3*a*). However, it should be noted that the presence of the second wall has little effect on the torque for $0 \leqslant s \leqslant 0{\cdot}3$. For $s > 0{\cdot}3$ the torque rises sharply especially at close spacings.

Figure 3(*c*) shows the torque acting on a sphere translating parallel to the walls or the force on a sphere which is rotating about an axis parallel to the walls. The value of F_x^r and T_y^t is zero at $s = 0{\cdot}5$ and becomes infinite as the sphere approaches one of the walls. It is interesting to note that the F_x^r and T_y^t coefficients change sign indicating that there is a second position other than midway between the two walls for which a sphere translating parallel to the walls will experience no torque or a sphere rotating about an axis parallel to the walls will experience no force. To help understand this intriguing behaviour we have plotted the velocity field in the plane $y = 0$ for both flow problems in figures 4(*a*, *b*) using equation (2.23) for the geometry $d/2a = 3$, $s = \frac{1}{3}$. This geometry corresponds to the maximum negative value of F_x^r and T_y^t for the curve $d/2a = 3$ shown in figure 3(*c*). The velocity vectors shown with arrowheads have been drawn to scale and show the magnitude and direction of the fluid motion. For cases where the magnitude of the velocity is too small to be visible on the scale shown the direction of the fluid motion is shown by a straight line without an arrow at the indicated point. Figure 4(*a*) shows the velocity field for a sphere translating between two walls with no rotation. Intuitively, one would expect that the net torque acting on the sphere by the fluid would be counter-clockwise since the sphere would

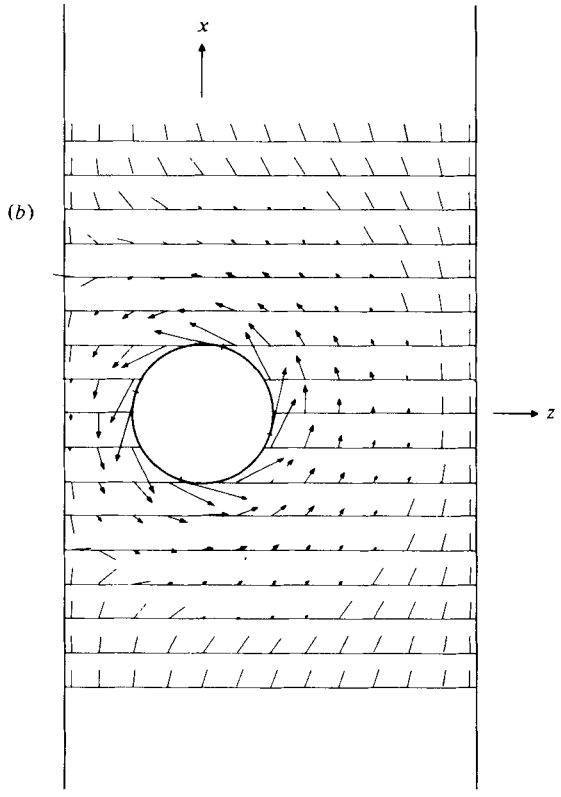

FIGURE 4. (*a*) Velocity field induced by the translation of a sphere parallel to two plane walls. (*b*) Velocity field induced by the rotation of a sphere about an axis parallel to two plane parallel walls. $d/2a = 3$, $s = \frac{1}{3}$.

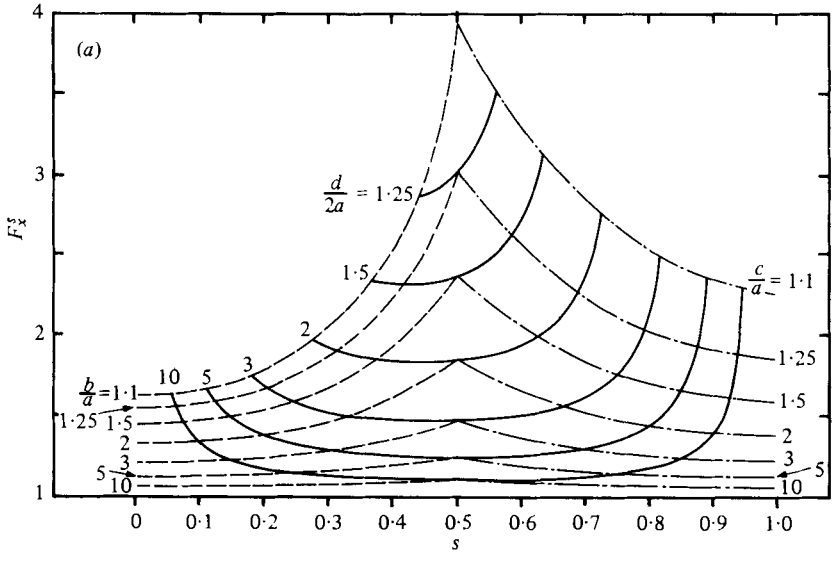

FIGURE 5 (*a*). For legend see p. 777.

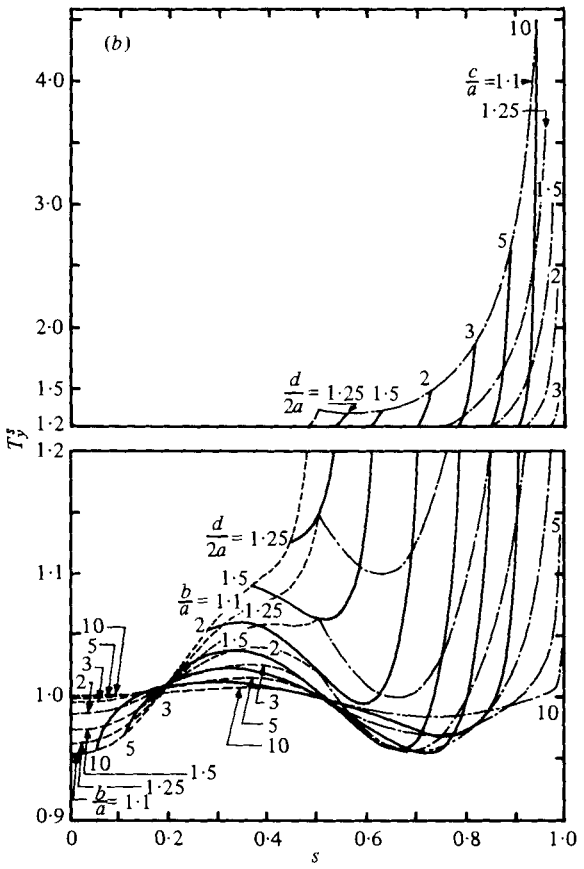

FIGURE 5. (*a*) Force and (*b*) torque on a rigidly held sphere in simple shear flow between two plane parallel walls induced by the motion of the wall at $z = c$. ——, $d/2a$ = constant; – – – –, b/a = constant; — · — · —, c/a = constant.

tend to roll along the nearer wall. However, a separated region of closed streamlines and relatively stagnant fluid forms near the wall which is further removed from the sphere. This stagnant region, which possesses a small clockwise circulation, obstructs the flow near the more distant wall and causes the shear stress on this side of the sphere to increase. The net effect is a small clockwise torque.

Figure 4(*b*) shows the velocity field induced by the rotation of a sphere about an axis parallel to the confining walls for the same geometry as shown in figure 4(*a*). There are two stagnation points on the nearer wall in the plane $y = 0$, one fore and one aft of the sphere. A stagnation streamline is attached normal to the wall at these points which encloses the sphere. Within this separated region, the fluid circulates about the sphere in closed streamlines. Outside the separated region, the fluid flows toward the positive-x direction. The reason for the negative force exerted by the fluid on the sphere is not readily obvious from the figure, but can be deduced from the balance of pressure and viscous stresses on the surface of the sphere. For small values of s the viscous stresses on the near wall dominate and produce a thrust in the positive-x direction. For larger values of s as the sphere moves toward the centre of the channel

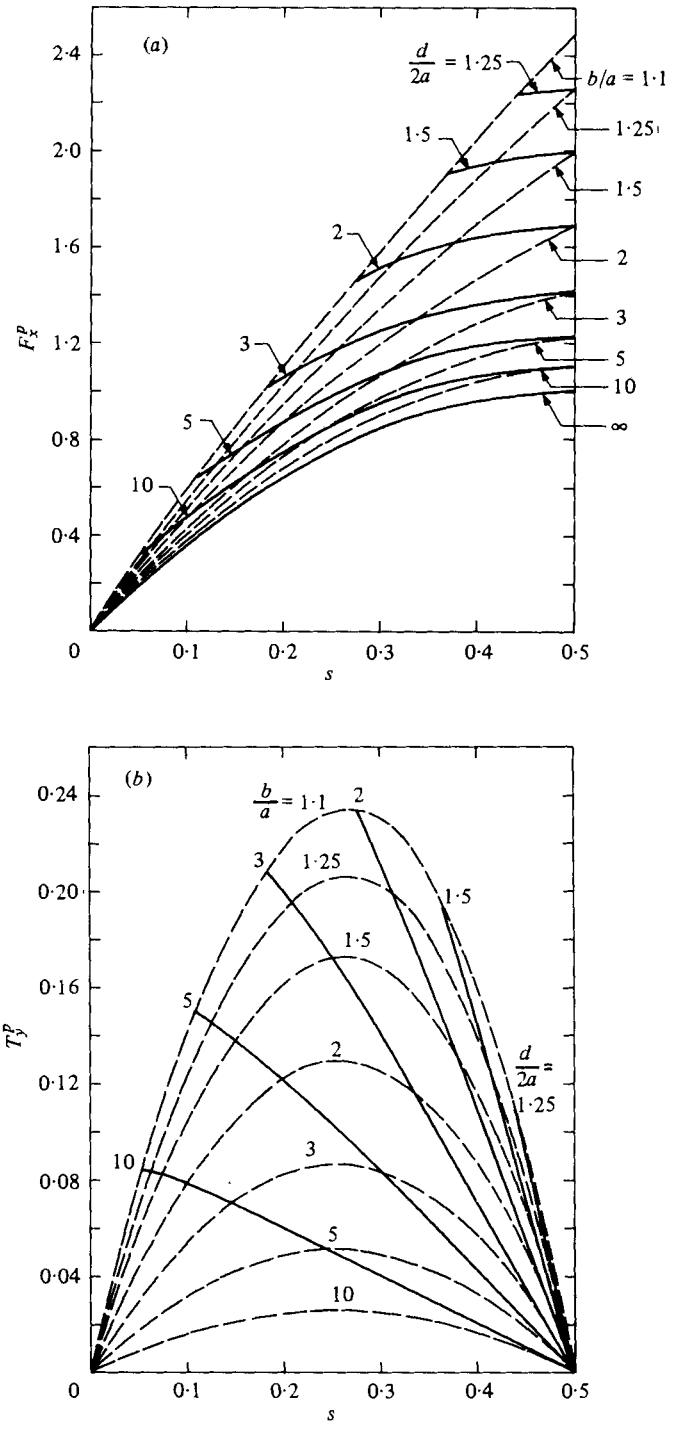

FIGURE 6. (*a*) Force and (*b*) torque on a rigidly held sphere in two-dimensional Poiseuille flow between two stationary walls. ——, $d/2a$ = constant; – – – –, b/a = constant.

the asymmetry of the pressure field fore and aft of the sphere is more important and causes a drag in the negative-x direction.

Figure 5(a) shows the force acting on a rigidly held sphere in Couette flow induced by the motion of the boundary at $z = c$ parallel to itself. For a fixed wall-to-wall spacing $d/2a$, minimum drag occurs for $s < 0{\cdot}5$ at close wall-to-wall spacings and near $s = 0{\cdot}5$ at large spacings. Figure 5(b) shows the torque acting on the sphere in Couette flow. At sufficiently large values of $d/2a$ the torque is observed to increase, then decrease, and then sharply approach infinity as the sphere approaches the moving wall.

Figures 6a, b show similar results for the force and torque acting on a sphere in two-dimensional Poiseuille flow between two stationary walls. The force acting on the sphere decreases with increasing values of $d/2a$ and approaches the parabolic curve shown for $d/2a = \infty$. The sphere experiences the maximum drag force when it is located midway between the two walls. Figure 6(b) shows that the torque is zero at the centre-line due to symmetry and increases almost linearly as the sphere approaches one of the walls. For a fixed value of b/a the maximum value of the torque occurs for s slightly larger than 0·25.

Solutions for any combination of the motions described in this paper may be obtained by a simple superposition of solutions. Thus for the most general case of parallel motion of a sphere between two plane walls, the force and torque exerted by the fluid on the sphere is given by

$$F_x = 6\pi\mu a[UF_x^t + a\Omega F_x^r + V_c F_x^p + bSF_x^s], \tag{4.12a}$$

$$T_y = 8\pi\mu a^2[UT_y^t + a\Omega T_y^r + V_c T_y^p + \tfrac{1}{2}aST_y^s], \tag{4.12b}$$

where values of the force and torque coefficients may be obtained from figures 3, 5 and 6 for a given geometry.

5. Application of the solution technique in future research

This paper has demonstrated that the boundary collocation technique previously used for quasi-steady unbounded multi-particle Stokes flows with planar symmetry may be applied to treat planar symmetric bounded flow problems with high accuracy. Among the unsolved problems which fall in this category are the arbitrary off-axis motion of a sphere in a circular cylinder, the tumbling of a spheroid near a planar boundary and the entrance motion of a sphere into a circular pore or a two-dimensional slit.

The success of the technique depends in large measure on the ability to perform the integral transform of the disturbances felt on the confining boundaries analytically. Many of the definite integrals which arise for the more common co-ordinate systems may be found in the literature for Fourier and Hankel transforms. A serious limitation of the technique is the long computation time required for the numerical evaluation of the inversion integrals. Extreme care must be taken in writing the program to save repeatedly needed calculations in memory in order to keep execution time at a minimum. Since the bulk of the computation time is used in the numerical evaluation of the integrals, it is vitally important that the integrating subroutine be as efficient as possible.

The authors wish to thank the National Science Foundation for supporting this research under grant ENG 75-19243 and The City University of New York Computer Center for the use of their facilities. The above work has been performed in partial fulfilment of the requirements for the Ph.D. degree of P. Ganatos from The School of Engineering of The City College of The City University of New York.

Appendix A

This appendix contains a listing of the starred $\mathscr{A}_n$, $\mathscr{B}_n$ and $\mathscr{C}_n$ functions contained in (2.16)

$$\mathscr{A}_n^*(\alpha,\beta,z_i) = -\frac{4}{\pi^2}\{n(2n-1)\,F_2(\alpha,\beta,z_i,n,1)+\tfrac{1}{2}(n-2) \times [F_2(\alpha,\beta,z_i,n-1,2)-F_2(\beta,\alpha,z_i,n-1,2)] -\tfrac{1}{2}n(n+1)\,(n-2)\,F_1(\alpha,\beta,z_i,n-1,0)\}, \tag{A 1}$$

$$\mathscr{B}_n^*(\alpha,\beta,z_i) = -\frac{4}{\pi^2}\{-\tfrac{1}{2}[F_2(\alpha,\beta,z_i,n+1,2)-F_2(\beta,\alpha,z_i,n+1,2)] +\tfrac{1}{2}n(n+1)\,F_1(\alpha,\beta,z_i,n+1,0)\}, \tag{A 2}$$

$$\mathscr{C}_n^*(\alpha,\beta,z_i) = -\frac{4}{\pi^2}\{\tfrac{1}{2}[F_2(\alpha,\beta,z_i,n,2)-F_2(\beta,\alpha,z_i,n,2)] +\tfrac{1}{2}n(n+1)\,F_1(\alpha,\beta,z_i,n,0)\}; \tag{A 3}$$

$$\mathscr{A}_n^{**}(\alpha,\beta,z_i) = -\frac{4}{\pi^2}[n(2n-1)\,F_3(\alpha,\beta,z_i,n,1)+(n-2)\,F_3(\alpha,\beta,z_i,n-1,2)], \tag{A 4}$$

$$\mathscr{B}_n^{**}(\alpha,\beta,z_i) = \frac{4}{\pi^2}F_3(\alpha,\beta,z_i,n+1,2), \tag{A 5}$$

$$\mathscr{C}_n^{**}(\alpha,\beta,z_i) = -\frac{4}{\pi^2}F_3(\alpha,\beta,z_i,n,2); \tag{A 6}$$

$$\mathscr{A}_n^{***}(\alpha,\beta,z_i) = -\frac{4}{\pi^2}[n(2n-1)\,z_i\,F_4(\alpha,\beta,z_i,n,1)-(n+1)\,(n-z)\,F_4(\alpha,\beta,z_i,n-1,1)], \tag{A 7}$$

$$\mathscr{B}_n^{***}(\alpha,\beta,z_i) = \frac{4}{\pi^2}nF_4(\alpha,\beta,z_i,n+1,1), \tag{A 8}$$

$$\mathscr{C}_n^{***}(\alpha,\beta,z_i) = \frac{4}{\pi^2}F_4(\alpha,\beta,z_i,n,1). \tag{A 9}$$

Appendix B

This appendix contains a summary of the formulae used in performing the inner set of integrals required by (2.22). These formulae were obtained using results and general formulae for Fourier transforms found in Erdelyi *et al.* (1954).

In the formulae which follow, a and b are positive constants, $u = (a^2+b^2)^{\frac{1}{2}}$ and J_0 and J_1 are Bessel functions of the first kind of order 0 and 1 respectively.

$$\int_0^{\frac{1}{2}\pi} \cos(a\cos\gamma)\cos(b\sin\gamma)\,d\gamma = \frac{\pi}{2}J_0(u), \tag{B 1}$$

$$\int_0^{\frac{1}{2}\pi} \cos^2\gamma\cos(a\cos\gamma)\cos(b\sin\gamma)\,d\gamma = \frac{\pi}{2u^2}\left[a^2J_0(u)+\frac{b^2-a^2}{u}J_1(u)\right], \tag{B 2}$$

$$\int_0^{\frac{1}{2}\pi} \cos\gamma\sin\gamma\sin(a\cos\gamma)\sin(b\sin\gamma)\,d\gamma = -\frac{\pi}{2}\frac{ab}{u^2}\left[J_0(u)-\frac{2}{u}J_1(u)\right], \tag{B 3}$$

$$\int_0^{\frac{1}{2}\pi} \cos\gamma\sin(a\cos\gamma)\cos(b\sin\gamma)\,d\gamma = \frac{\pi}{2}\frac{a}{u}J_1(u). \tag{B 4}$$

Appendix C

This appendix contains a listing of the primed $\mathscr{A}_n$, $\mathscr{B}_n$ and $\mathscr{C}_n$ functions contained in (2.24).

$$\mathscr{A}'_n = \int_0^\infty \{G_5(\eta)H_1(-b)-G_5(\sigma)H_1(c)+G_6(\sigma,\eta)H_2(-b)-G_6(\eta,\sigma)H_2(c) + G_1(\sigma,\eta)H_3(-b)-G_1(\eta,\sigma)H_3(c)\}\,d\kappa, \tag{C 1a}$$

$$\mathscr{B}'_n = \int_0^\infty \{G_5(\eta)H_4(-b)-G_5(\sigma)H_4(c)+G_6(\sigma,\eta)H_5(-b)-G_6(\eta,\sigma)H_5(c) + G_1(\sigma,\eta)H_6(-b)-G_1(\eta,\sigma)H_6(c)\}\,d\kappa, \tag{C 1b}$$

$$\mathscr{C}'_n = \int_0^\infty \{G_5(\eta)H_7(-b)-G_5(\sigma)H_7(c)+G_6(\sigma,\eta)H_8(-b)-G_6(\eta,\sigma)H_8(c) + G_1(\sigma,\eta)H_9(-b)-G_1(\eta,\sigma)H_9(c)\}\,d\kappa, \tag{C 1c}$$

$$\mathscr{A}''_n = \int_0^\infty \{G_6(\sigma,\eta)H_{10}(-b)-G_6(\eta,\sigma)H_{10}(c)+G_3(\sigma,\eta)H_{11}(-b)-G_3(\eta,\sigma)H_{11}(c) + G_1(\sigma,\eta)H_{12}(-b)-G_1(\eta,\sigma)H_{12}(c)\}\,d\kappa, \tag{C 1d}$$

$$\mathscr{B}''_n = \int_0^\infty \{G_6(\sigma,\eta)H_{13}(-b)-G_6(\eta,\sigma)H_{13}(c)+G_3(\sigma,\eta)H_{14}(-b)-G_3(\eta,\sigma)H_{14}(c) + G_1(\sigma,\eta)H_{15}(-b)-G_1(\eta,\sigma)H_{15}(c)\}\,d\kappa, \tag{C 1e}$$

$$\mathscr{C}''_n = \int_0^\infty \{G_6(\sigma,\eta)H_{16}(-b)-G_6(\eta,\sigma)H_{16}(c)+G_3(\sigma,\eta)H_{17}(-b)-G_3(\eta,\sigma)H_{17}(c) + G_1(\sigma,\eta)H_{18}(-b)-G_1(\eta,\sigma)H_{18}(c)\}\,d\kappa, \tag{C 1f}$$

$$\mathscr{A}'''_n = \int_0^\infty \{G_2(\sigma,\eta)H_{19}(-b)-G_2(\eta,\sigma)H_{19}(c)+G_4(\sigma,\eta)H_{20}(-b)-G_4(\eta,\sigma)H_{20}(c)\}\,d\kappa, \tag{C 1g}$$

$$\mathscr{B}'''_n = \int_0^\infty \{G_2(\sigma,\eta)H_{21}(-b)-G_2(\eta,\sigma)H_{21}(c)+G_4(\sigma,\eta)H_{22}(-b) - G_4(\eta,\sigma)H_{22}(c)\}\,d\kappa, \tag{C 1h}$$

$$\mathscr{C}_n''' = \int_0^\infty \{G_2(\sigma,\eta)\,H_{23}(-b) - G_2(\eta,\sigma)\,H_{23}(c) + G_4(\sigma,\eta)\,H_{24}(-b) - G_4(\eta,\sigma)\,H_{24}(c)\}\,d\kappa, \tag{C 1i}$$

where

$$H_1(z_i) = -n(2n-1)\,z_i^3 J_0(\kappa\rho)\,B_{n,1,1,0}(z_i) + n(2n-1)\frac{z_i^2}{\rho^2}B_1 B_{n,1,2,1}(z_i) - \tfrac{1}{2}(n-2)\,(y^2-x^2)\,B_2 B_{n-1,2,2,3}(z_i) + \tfrac{1}{2}n(n+1)\,(n-2)\,J_0(\kappa\rho)\,B_{n-1,0,0,1}(z_i), \tag{C 2a}$$

$$H_2(z_i) = \{-n(2n-1)\,z_i^2[B_{n,1,1,0}(z_i) - B_{n,1,2,1}(z_i)] + \tfrac{1}{2}(n-2)\,z_i^2 B_{n-1,2,2,1}(z_i) + \tfrac{1}{2}n(n+1)\,(n-2)\,B_{n-1,0,0,1}(z_i)\}\frac{B_1}{\rho^2}, \tag{C 2b}$$

$$H_3(z_i) = \kappa z_i^2[-n(2n-1)\,z_i\,B_{n,1,1,0}(z_i) + (n+1)\,(n-2)\,B_{n-1,1,1,0}(z_i)]\frac{B_1}{\rho^2}, \tag{C 2c}$$

$$H_4(z_i) = \tfrac{1}{2}[(y^2-x^2)\,B_2 B_{n+1,2,2,3}(z_i) - n(n+1)\,J_0(\kappa\rho)\,B_{n+1,0,0,1}(z_i)], \tag{C 2d}$$

$$H_5(z_i) = -\tfrac{1}{2}[z_i^2 B_{n+1,2,2,1}(z_i) + n(n+1)\,B_{n+1,0,0,1}(z_i)]\frac{B_1}{\rho^2}, \tag{C 2e}$$

$$H_6(z_i) = n\frac{\kappa z_i^2}{\rho^2}B_1 B_{n+1,1,1,0}(z_i), \tag{C 2f}$$

$$H_7(z_i) = -\tfrac{1}{2}[(y^2-x^2)\,B_2 B_{n,2,2,3}(z_i) + n(n+1)\,J_0(\kappa\rho)\,B_{n,0,0,1}(z_i)], \tag{C 2g}$$

$$H_8(z_i) = \tfrac{1}{2}[z_i^2 B_{n,2,2,1}(z_i) - n(n+1)\,B_{n,0,0,1}(z_i)]\frac{B_1}{\rho^2}, \tag{C 2h}$$

$$H_9(z_i) = \kappa z_i^2 B_{n,1,1,0}(z_i)\frac{B_1}{\rho^2}, \tag{C 2i}$$

$$H_{10}(z_i) = xyB_2\left[-n(2n-1)\,B_{n,1,1,2}(z_i) - \tfrac{1}{2}(n-2)\,B_{n-1,2,2,3}(z_i) + \frac{1}{2z_i^2}n(n+1)\,(n-2)\,B_{n-1,0,0,3}(z_i)\right], \tag{C 2j}$$

$$H_{11}(z_i) = xyB_2[n(2n-1)\,B_{n,1,2,3}(z_i) + (n-2)\,B_{n-1,2,2,3}(z_i)], \tag{C 2k}$$

$$H_{12}(z_i) = \kappa xyB_2[-n(2n-1)\,z_i\,B_{n,1,1,2}(z_i) + (n+1)\,(n-2)\,B_{n-1,1,1,2}(z_i)], \tag{C 2l}$$

$$H_{13}(z_i) = \tfrac{1}{2}xyB_2\left[B_{n+1,2,2,3}(z_i) - n(n+1)\frac{1}{z_i^2}B_{n+1,0,0,3}(z_i)\right], \tag{C 2m}$$

$$H_{14}(z_i) = -xyB_2 B_{n+1,2,2,3}(z_i), \tag{C 2n}$$

$$H_{15}(z_i) = n\kappa xyB_2 B_{n+1,1,1,2}(z_i), \tag{C 2o}$$

$$H_{16}(z_i) = -\tfrac{1}{2}xyB_2\left[B_{n,2,2,3}(z_i) + n(n+1)\frac{1}{z_i^2}B_{n,0,0,3}(z_i)\right], \tag{C 2p}$$

$$H_{17}(z_i) = xyB_2 B_{n,2,2,3}(z_i), \tag{C 2q}$$

$$H_{18}(z_i) = \kappa xyB_2 B_{n,1,1,2}(z_i), \tag{C 2r}$$

$$H_{19}(z_i) = -x\frac{J_1(\kappa\rho)}{\kappa^2\rho}\left\{n(2n-1)\left[B_{n,1,1,2}(z_i)-B_{n,1,2,3}(z_i)\right]\right.$$
$$\left.-\tfrac{1}{2}(n-2)\,B_{n-1,2,2,3}(z_i)-\tfrac{1}{2}n(n+1)\,(n-2)\frac{1}{z_i^2}B_{n-1,0,0,3}(z_i)\right\}, \tag{C 2s}$$

$$H_{20}(z_i) = -x\frac{J_1(\kappa\rho)}{\kappa\rho}\left[n(2n-1)\,z_i B_{n,1,1,2}(z_i)-(n+1)\,(n-2)\,B_{n-1,1,1,2}(z_i)\right], \tag{C 2t}$$

$$H_{21}(z_i) = -\tfrac{1}{2}x\frac{J_1(\kappa\rho)}{\kappa^2\rho}\left[B_{n+1,2,2,3}(z_i)+n(n+1)\frac{1}{z_i^2}B_{n+1,0,0,3}(z_i)\right], \tag{C 2u}$$

$$H_{22}(z_i) = nx\frac{J_1(\kappa\rho)}{\kappa\rho}B_{n+1,1,1,2}(z_i), \tag{C 2v}$$

$$H_{23}(z_i) = \tfrac{1}{2}x\frac{J_1(\kappa\rho)}{\kappa^2\rho}\left[B_{n,2,2,3}(z_i)-n(n+1)\frac{1}{z_i^2}B_{n,0,0,3}(z_i)\right], \tag{C 2w}$$

$$H_{24}(z_i) = x\frac{J_1(\kappa\rho)}{\kappa\rho}B_{n,1,1,2}(z_i). \tag{C 2x}$$

Here

$$B_1 = x^2J_0(\kappa\rho)+(y^2-x^2)\frac{J_1(\kappa\rho)}{\kappa\rho}, \tag{C 3a}$$

$$B_2 = \frac{1}{\kappa^2\rho^2}\left[J_0(\kappa\rho)-2\frac{J_1(\kappa\rho)}{\kappa\rho}\right], \tag{C 3b}$$

$$\rho = (x^2+y^2)^{\frac{1}{2}} \tag{C 4}$$

and

$$B_{n,m,j,l}(z_i) = \sum_{q=0}^{[\frac{1}{2}n]} S_{nmq}(z_i)\,(\kappa|z_i|)^{n-q+l-\frac{1}{2}}K_{n-q-j-\frac{1}{2}}(\kappa|z_i|), \tag{C 5}$$

where J_ν is the Bessel function of the first kind, K_ν is the modified Bessel function of the second kind and $S_{nmq}(z_i)$ is defined by (2.15).

REFERENCES

Bretherton, F. P. 1962 *J. Fluid Mech.* **14**, 284.

Erdelyi, A., Magnus, W., Oberhettinger, F. & Tricomi, F. G. 1954 *Tables of Integral Transforms*, vols. 1 and 2, McGraw-Hill.

Faxen, H. 1923 *Arkiv. Mat. Astron. Fys.* **17**, no. 27.

Ganatos, P. 1979 Ph.D. dissertation, City University of New York.

Ganatos, P., Pfeffer, R. & Weinbaum, S. 1978 *J. Fluid Mech.* **84**, 79.

Ganatos, P., Weinbaum, S. & Pfeffer, R. 1980 *J. Fluid Mech.* **99**, 739–753.

Goldman, A. J., Cox, R. G. & Brenner, H. 1967*a* *Chem. Engng Sci.* **22**, 637.

Goldman, A. J., Cox, R. G. & Brenner, H. 1967*b* *Chem. Engng Sci.* **22**, 653.

Halow, J. S. & Wills, G. B. 1970 *A.I.Ch.E. J.* **16**, 281.

Happel, J. & Brenner, H. 1973 *Low Reynolds Number Hydrodynamics*, 2nd edn. Noordhoff.

Ho, B. P. & Leal, L. G. 1974 *J. Fluid Mech.* **65**, 365.

Lamb, H. 1945 *Hydrodynamics*, 6th edn. Dover.

O'Neill, M. E. 1964 *Mathematika* **11**, 67.

Wakiya, S. 1956 *Res. Rep. Fac. Engng, Niigata University (Japan)*, **5**, 1.